AMERICAN SOCIETY FOR MICROBIOLOGY | Infection and Immunity®

BACTERIAL INFECTIONS

Link between Heterotrophic Carbon Fixation and Virulence in the Porcine Lung Pathogen *Actinobacillus pleuropneumoniae*

Sarah A. Konze,[a] Wolf-Rainer Abraham,[b] Elke Goethe,[c] Esther Surges,[b] Marcel M. M. Kuypers,[d] Doris Hoeltig,[e] Jochen Meens,[c] Charlotte Vogel,[f] Meike Stiesch,[g] Peter Valentin-Weigand,[c] Gerald-F. Gerlach,[c] Falk F. R. Buettner[a]

[a]Institute of Clinical Biochemistry, Hannover Medical School, Hannover, Germany
[b]Helmholtz Center for Infection Research, Chemical Microbiology, Braunschweig, Germany
[c]Institute for Microbiology, Department of Infectious Diseases, University of Veterinary Medicine Hannover, Foundation, Hannover, Germany
[d]Department of Biogeochemistry, Max Planck Institute for Marine Microbiology, Bremen, Germany
[e]Clinic for Swine and Small Ruminants and Forensic Medicine and Ambulatory Services, University of Veterinary Medicine Hannover, Foundation, Hannover, Germany
[f]Department of Biometry, Epidemiology and Information Processing, University of Veterinary Medicine Hannover, Foundation, Hannover, Germany
[g]Department of Prosthetic Dentistry and Materials Sciences, Hannover Medical School, Hannover, Germany

ABSTRACT *Actinobacillus pleuropneumoniae* is a capnophilic pathogen of the porcine respiratory tract lacking enzymes of the oxidative branch of the tricarboxylic acid (TCA) cycle. We previously claimed that *A. pleuropneumoniae* instead uses the reductive branch in order to generate energy and metabolites. Here, we show that bicarbonate and oxaloacetate supported anaerobic growth of *A. pleuropneumoniae*. Isotope mass spectrometry revealed heterotrophic fixation of carbon from stable isotope-labeled bicarbonate by *A. pleuropneumoniae*, which was confirmed by nanoscale secondary ion mass spectrometry at a single-cell level. By gas chromatography-combustion-isotope ratio mass spectrometry we could further show that the labeled carbon atom is mainly incorporated into the amino acids aspartate and lysine, which are derived from the TCA metabolite oxaloacetate. We therefore suggest that carbon fixation occurs at the interface of glycolysis and the reductive branch of the TCA cycle. The heme precursor δ-aminolevulinic acid supported growth of *A. pleuropneumoniae*, similar to bicarbonate, implying that anaplerotic carbon fixation is needed for heme synthesis. However, deletion of potential carbon-fixing enzymes, including PEP-carboxylase (PEPC), PEP-carboxykinase (PEPCK), malic enzyme, and oxaloacetate decarboxylase, as well as various combinations thereof, did not affect carbon fixation. Interestingly, generation of a deletion mutant lacking all four enzymes was not possible, suggesting that carbon fixation in *A. pleuropneumoniae* is an essential metabolic pathway controlled by a redundant set of enzymes. A double deletion mutant lacking PEPC and PEPCK was not impaired in carbon fixation *in vitro* but showed reduction of virulence in a pig infection model.

KEYWORDS *Actinobacillus pleuropneumoniae*, carbon fixation, heme, oxaloacetate, phosphoenolpyruvate, swine, virulence

The *Pasteurellaceae* member *Actinobacillus pleuropneumoniae* is a capnophilic (CO_2-"loving") Gram-negative bacterium that causes porcine pleuropneumonia, a highly infectious disease occurring in pigs worldwide (1). *A. pleuropneumoniae* is transferred by droplet infection between pigs and colonizes the respiratory epithelium. The pathogen can persist on tonsils and lung epithelium and in sequestered purulent lesions of the lung. Clinically healthy-appearing animals having a persistent infection are the major sources for transmission of the pathogen (2, 3).

Virulence of *A. pleuropneumoniae* depends on anaerobic metabolism, as suggested by our previous findings that deletion of the anaerobic regulatory factors ArcA and FNR

Citation Konze SA, Abraham W-R, Goethe E, Surges E, Kuypers MMM, Hoeltig D, Meens J, Vogel C, Stiesch M, Valentin-Weigand P, Gerlach G-F, Buettner FFR. 2019. Link between heterotrophic carbon fixation and virulence in the porcine lung pathogen *Actinobacillus pleuropneumoniae*. Infect Immun 87:e00768-18. https://doi.org/10.1128/IAI.00768-18.

Editor Sabine Ehrt, Weill Cornell Medical College

Address correspondence to Falk F. R. Buettner, buettner.falk@mh-hannover.de.

Received 12 October 2018
Returned for modification 22 February 2019
Accepted 24 June 2019
Accepted manuscript posted online 8 July 2019
Published 21 August 2019

(HlyX) led to attenuation in infection of *A. pleuropneumoniae* (4–6). It has been further proposed that *A. pleuropneumoniae* uses the reductive branch of the tricarboxylic acid (TCA) cycle during anaerobic respiration, and fumarate reductase was shown to be an essential determinant of virulence (7). The *A. pleuropneumoniae* genome (NCBI accession number NC_010939.1) does not encode homologues of citrate synthase, aconitase, and isocitrate dehydrogenase, which are enzymes of the oxidative branch of the TCA cycle. Thus, we have previously assumed that metabolites of glycolysis enter the TCA cycle via the reductive branch (7). The conversion of glycolytic C_3 compounds into C_4 metabolites of the reductive branch of the TCA cycle requires a carboxylation reaction at the phosphoenolpyruvate (PEP)-pyruvate-oxaloacetate node (8). Anaplerotic carboxylation in bacteria is generally mediated by PEP carboxylase (PEPC), pyruvate carboxylase, or PEP carboxytransphosphorylase. Of these, only PEPC is encoded by *A. pleuropneumoniae*, and it is considered to catalyze the highly exergonic heterotrophic carboxylation of PEP to oxaloacetate (8). Further enzymes working at the PEP-pyruvate-oxaloacetate node that are encoded by *A. pleuropneumoniae* include PEP carboxykinase (PEPCK), malic acid enzyme (MAE), and oxaloacetate decarboxylase complex (OAD). PEPCK and MAE catalyze both C_3-carboxylation as well as C_4-decarboxylation reactions, but in most bacterial species they are responsible for the latter reaction, whereas OAD is generally considered to catalyze only the decarboxylation of oxaloacetate (8). The *A. pleuropneumoniae* relatives *Mannheimia succiniciproducens* and *Actinobacillus succinogenes* are among the best succinate-producing bacterial species known, as they fix carbonate and produce succinic acid by fumarate reduction as part of a mixed-acid fermentation (9, 10). *M. succiniciproducens* possesses at least three enzymes that interconvert C_3 and C_4 compounds, namely, PEPC, PEPCK, and MAE (9), whereas *A. succinogenes* lacks PEPC (10), and in both species PEPCK is most important for succinic acid production (10, 11). This reaction not only fixes carbon but also provides additional ATP. In contrast, PEPC is most relevant for carbon fixation from CO_2 in *Escherichia coli* (12, 13) and in *Streptococcus suis* (14). However, flux analyses in *A. succinogenes* revealed that in addition to phosphoenolpyruvate, oxaloacetate, and malate, flux distribution between the C_3 and C_4 pathways can also occur via pyruvate. The highly reversible flux between pyruvate and malate/oxaloacetate is mediated through MAE and OAD. Of these, MAE is assumed to catalyze the energetically favored carboxylation of pyruvate to malate, but activity of OAD as a carboxylase cannot be ruled out (15, 16).

CO_2 can function as a signaling molecule influencing virulence of pathogenic bacteria (17). Accordingly, CO_2/bicarbonate was shown to affect transcription of virulence factors in several pathogenic species, including virulent *Bacilli* (18), *Enterococcus faecalis* (19), *Streptococcus pyogenes* (20), *Staphylococcus aureus* (21), and *Vibrio cholerae* (22). Bicarbonate and CO_2 comprise the major blood buffering system, with concentrations of bicarbonate around 13 mM in whole blood (23). Thus, it appears likely that pathogenic bacteria detect and respond to CO_2/bicarbonate in their mammalian hosts (24). However, the role of CO_2/bicarbonate as a carbon source for pathogenic bacteria has been poorly studied so far.

The lung is the main interface for CO_2 exchange between the body and the environment, and lung epithelial cells secrete bicarbonate, which is trapped in the mucus, where it contributes to mucus pH and viscosity (25). In order to study the importance of bicarbonate for *A. pleuropneumoniae*, we deleted enzymes catalyzing carboxylation or decarboxylation reactions at the interface of C_3 and C_4 pathways and analyzed carbon fixation and virulence of the deletion mutants. We showed that *A. pleuropneumoniae* can heterotrophically fix carbon from bicarbonate, and we provide evidence that this fixation appears at the PEP-pyruvate-oxaloacetate-malate node and is important for virulence.

RESULTS

Deletion of potential carboxylases in *A. pleuropneumoniae*. PEPC, PEPCK, MAE, and OAD of *A. succinogenes* and/or *M. succiniciproducens* were shown to interconvert C_3 and C_4 compounds (9, 16), and homologues of these enzymes are encoded by the genome of *A. pleuropneumoniae* serovar 7 strain AP76 (NCBI accession no. PRJNA29909)

by *pepC*, *pckA*, *maeB*, and *oadA*, respectively. In order to study the importance of PEPC, PEPCK, MAE, and the α subunit of OAD (which contains the carboxyltransferase activity) for heterotrophic carbon fixation in *A. pleuropneumoniae*, isogenic and unmarked deletion mutants of *pepC*, *pckA*, *maeB*, and *oadA* and multiple deletion mutants with different combinations of deletions in these genes were constructed by allelic exchange of the respective wild-type gene with in-frame truncated versions (Table 1; also see Fig. S1 in the supplemental material). By the genomic manipulations most amino acids of the respective proteins were deleted. The deletion comprised amino acids 9 to 856 (of 879 amino acids) for PEPC, 14 to 526 (of 536 amino acids) for PEPCK, 16 to 404 (of 422 amino acids) for MAE, and 29 to 588 (of 600 amino acids) for the α subunit of OAD. Therefore, no residual activity of the truncated versions of the enzymes was expected. The resulting *A. pleuropneumoniae* deletion mutants were confirmed by PCR (Fig. S2).

We deleted *pepC*, *pckA*, and *maeB* successively (leading to the Δ*pepC* Δ*pckA* Δ*maeB* strain) as well as *oadA*, *maeB*, and *pckA* successively (leading to the Δ*oadA* Δ*maeB* Δ*pckA* strain) in *A. pleuropneumoniae*, applying our well-established single-step transconjugation system. However, we did not succeed in deleting *oadA* in the Δ*pepC* Δ*pckA* Δ*maeB* triple mutant, and we could not delete *pepC* in the Δ*oadA* or Δ*oadA* Δ*maeB* mutant even after several rounds and testing of hundreds of clones. Taken together, mutants of *A. pleuropneumoniae* with all combinations of deletions in *pepC*, *pckA*, *maeB*, and *oadA* could be successfully generated, with the exception of any mutant carrying combined deletions of *pepC* and *oadA*.

Bicarbonate, oxaloacetate, and δ-aminolevulinic acid support growth of *A. pleuropneumoniae*. We had observed that growth of *A. pleuropneumoniae* in closed tubes was considerably impaired when we used autoclaved instead of sterile filtered PPLO medium, and this effect was mostly restored when we let the medium cool down before sealing the bottle (data not shown). Thus, we concluded that the heating has not destroyed essential ingredients of the medium but rather led to removal of dissolved gases. Interestingly, supplementation of autoclaved PPLO medium with sodium bicarbonate ($NaHCO_3$) significantly augmented growth of *A. pleuropneumoniae*. Upon 6 h of growth, optical density at 600 nm (OD_{600}) values were maximal for cultures supplemented with 5 mM $NaHCO_3$ (Fig. 1A). In addition to the *A. pleuropneumoniae* wild type, similar supportive effects of 5 mM $NaHCO_3$ on growth were also observed for all deletion mutants generated in this study, and 2 mM oxaloacetic acid showed supportive effects on growth similar to those of bicarbonate (Fig. 1B and Fig. S3). We hypothesized that bicarbonate is fixed at the PEP-pyruvate-oxaloacetate node and tested a panel of downstream metabolites for whether they could restore growth in the absence of bicarbonate. We applied the *A. pleuropneumoniae* wild type as a control, the Δ*pepC* Δ*pckA* mutant, which was used in the infection experiments (see below), as well as the Δ*pepC* Δ*pckA* Δ*maeB* and Δ*oadA* Δ*maeB* Δ*pckA* triple mutants that cover all other generated mutant strains. Addition of oxaloacetic acid supported growth of all tested strains (Fig. 1C). The oxaloacetate-derived amino acid aspartate, for which we observed the highest incorporation levels of carbon from bicarbonate (see below), did not support growth. Subsequent metabolites of the TCA cycle, like malate or fumarate, slightly restored growth, whereas the nonproteinogenic amino acid δ-aminolevulinic acid (ALA) significantly augmented growth of all tested strains in the absence of bicarbonate. ALA is the first metabolite in the core path of uroporphyrinogen III synthesis, which is the precursor of heme (26). However, hemin did not show any supportive effect on growth, but its poor solubility prevented its application at concentrations similar to those of the other compounds (Fig. 1C).

***A. pleuropneumoniae* can fix carbon from bicarbonate.** By nano-scale secondary ion mass spectrometry (nanoSIMS) analysis, we could show at the single-cell level that wild-type *A. pleuropneumoniae* is able to incorporate ^{13}C upon growth in $NaH^{13}CO_3$-supplemented medium (Fig. 2A and B). In order to scrutinize this observation, we performed element analysis-combustion-isotope ratio mass spectrometry (EA/C/IRMS),

TABLE 1 Bacterial strains, plasmids, and primers used in this study

Strain, plasmid, or primer	Characteristic(s) or sequence[c] (3′–5′)
Strains	
A. pleuropneumoniae	
WT	*A. pleuropneumoniae* serotype 7 isolate AP76 (52)
Δ*pepC*[a]	Unmarked *pepC* deletion mutant of *A. pleuropneumoniae* WT
Δ*pckA*[a]	Unmarked *pckA* deletion mutant of *A. pleuropneumoniae* WT
Δ*maeB*[a]	Unmarked *maeB* deletion mutant of *A. pleuropneumoniae* WT
Δ*oadA*[a]	Unmarked *oadA* deletion mutant of *A. pleuropneumoniae* WT
Δ*pepC* Δ*pckA*[a]	Unmarked *pckA* deletion mutant of *A. pleuropneumoniae* Δ*pepC* strain
Δ*oadA* Δ*pckA*[a]	Unmarked *pckA* deletion mutant of *A. pleuropneumoniae* Δ*oadA* strain
Δ*oadA* Δ*maeB*[a]	Unmarked *maeB* deletion mutant of *A. pleuropneumoniae* Δ*oadA* strain
Δ*pepC* Δ*pckA* Δ*maeB*[a]	Unmarked *maeB* deletion mutant of *A. pleuropneumoniae* Δ*pepC* Δ*pckA* strain
Δ*oadAC* Δ*maeB* Δ*pckA*[a]	Unmarked *pckA* deletion mutant of *A. pleuropneumoniae* Δ*oadA* Δ*maeB* strain
E. coli	
β2155	*thrB1004 pro thi strA hsdS lacZ*ΔM15 (F′ *lacZ*ΔM15 *laqI*^{q} *traD36 proA*$^+$ *proB*$^+$)Δ*dap*::*erm* (Erm^r) *recA*::*RPA-2-tet* (Tcr)::Mu-km (Kan^r) λ *pir* (53)
Plasmids	
pCR2.1-TOPO	*E. coli* cloning vector for cloning of *Taq* polymerase-amplified PCR products (Thermo Fisher Scientific)
pEMOC2	Transconjugation vector based on pBluescript SK with *mobRP4*, a polycloning site, Cm^r, and transcriptional fusion of the *omlA* promotor with the *sacB* gene (accession no. AJ868288 [54])
pPEP800[a]	pCR2.1-TOPO containing PCR product of o_pepC_3 and o_pepC_4
pPEP810[a]	pCR2.1-TOPO containing PCR product of o_pepC_1 and o_pepC_2
pPEP820[a]	Ligation product of pPEP810 and pPEP800 after digestion with PspOMI and BsmBI
pPCK800[a]	pCR2.1-TOPO containing PCR product of o_pckA_3 and o_pckA_4
pPEP700[a]	Final vector for conjugation; ligation product of the truncated *pepC* ORF excised from pPEP820 and the vector pEMOC2, both digested with NotI and PspOMI
pPCK810[a]	pCR2.1-TOPO containing PCR product of o_pepC_1 and o_pepC_2
pPCK820[a]	Ligation product of pPEP810 and pPEP800 after digestion with PspOMI and BsmBI
pPCK700[a]	Final vector for conjugation; ligation product of the truncated *pckA* ORF excised from pPCK820 and the vector pEMOC2, both digested with NotI and PspOMI
pMAE800[a]	pCR2.1-TOPO containing PCR product of o_maeB_3 and o_maeB_4
pMAE810[a]	pCR2.1-TOPO containing PCR product of o_maeB_1 and o_maeB2
pMAE820[a]	Ligation product of pMAE810 and pMAE800 after digestion with PspOMI and BsmBI
pMAE700[a]	Final vector for conjugation; ligation product of the truncated *maeB* ORF excised from pMAE820 and the vector pEMOC2, both digested with NotI and PspOMI
pOAD800[a]	pCR2.1-TOPO containing PCR product of o_oadA_3 and o_oadA_4
pOAD810[a]	pCR2.1-TOPO containing PCR product of o_oadA_1 and o_oadA2
pOAD820[a]	Ligation product of pOAD810 and pOAD800 after digestion with PspOMI and BsmBI
pOAD700[a]	Final vector for conjugation; ligation product of the truncated *oadA* ORF excised from pOAD820 and the vector pEMOC2, both digested with NotI and PspOMI
Primers (5′ to 3′)	
o_pepC_1[a]	ACGT**GGGCCC**TATGGCGGCAATTAACGGTG; fw; with PspOMI restriction site; pos. 576–555 upstream of *pepC* start codon
o_pepC_2[a]	ACGT**CGTCTC**GCATAGCGGAGTAGGGTTGAT; rev; with BsmBI site (underlined); pos. 5–24 of *pepC*
o_pepC_3[a]	ACGT**CGTCTC**CTATGCCGCAATTGGAACAAGCCTT; fw; with BsmBI site (underlined); pos. 2572–2591 of *pepC*
o_pepC_4[a]	ACGT**GCGGCCGC**CTTTGAGTGCATAGGACG; rev; with NotI site; pos. 836–855 downstream of *pepC* stop codon
o_pepC_5[a]	CCGTATCGGTATGCTGGAAA; fw; binding in deleted region of *pepC*
o_pckA_1[a]	GTAC**GGGCCC**CGTGCCGCATCATGTACTAA; fw; with PspOMI site; pos. 883–864 upstream of *pckA* start codon
o_pckA_2[a]	GTAC**CGTCTC**GTTTACCTAATTGTGCTAGTTCTTG; rev; with BsmBI site; pos. 19–38 of *pckA*
o_pckA_3[a]	GTAC**CGTCTC**GTAAAGCGTTAGTTGCGGCAG; fw; with BsmBI site; pos. 1578–1597 of *pckA*
o_pckA_4[a]	GTAC**GCGGCCGC**CAATTAATCCAAGATGCCGC; rev; with NotI site; pos. 699–718 downstream of *pckA* stop codon
o_pckA_5[a]	AAATTAGCGGGTACCGAACG; fw; binding in deleted region of *pckA*
o_maeB_1[a,b]	GTAC**GGGCCC**CGATCGATACCTTCCTGCTT; fw; with PspOMI site; pos. 864–845 upstream of *maeB* start codon
o_maeB_2[a]	GTAC**CGTCTC**TGTACCGGAAATTCGTGGAAGTC; rev; with BsmBI site; pos. 27–46 of *maeB*
o_maeB_3[a]	GTAC**CGTCTC**AGTACCGATTACCGATTGGGATGCG; fw; with BsmBI site; pos. 1216–1235 of *maeB*
o_maeB_4[a,b]	GTAC**GCGGCC**GCCAGACGTTATCTGGCACTCT; rev; with NotI site; pos. 707–726 downstream of *maeB* stop codon
o_maeB_5[a]	TATGTACCGGTCGTTCGGAT; fw; binding in deleted region of *maeB*
o_oadA_1[a,b]	GTACGGGCCCTGACTGCTCTATTCGCCATC; fw; with PspOMI restriction site; pos. 576–555 upstream of *pepC* start codon
o_oadA_2[a]	GTACCGTCTCGCGACACGTAGTCGTGTCGCAAACA; rev; with BsmBI site (underlined); pos. 5–24 of *pepC*
o_oadA_3[a]	GTACCGTCTCGGTCGTTGCCGTTGATCAAGT; fw; with BsmBI site (underlined); pos. 2572–2591 of *pepC*
o_oadA_4[a,b]	GTAC**GCGGCCGC**TGCGTAATTGCACCAT; rev; with NotI site; pos. 836–855 downstream of *pepC* stop codon
o_oadA_5[a]	ACCAACAGCAGAATCCGCTA; fw; binding in deleted region of *oadA*

[a]Strains, plasmids, or primers that were generated or designed in this study.
[b]These primers were modified for genotyping PCRs, i.e., bases for generation of restriction sites were omitted.
[c]Boldface letters in primer sequences indicate restriction sites. Abbreviations: fw, forward; rev, reverse; pos., position; ORF, open reading frame.

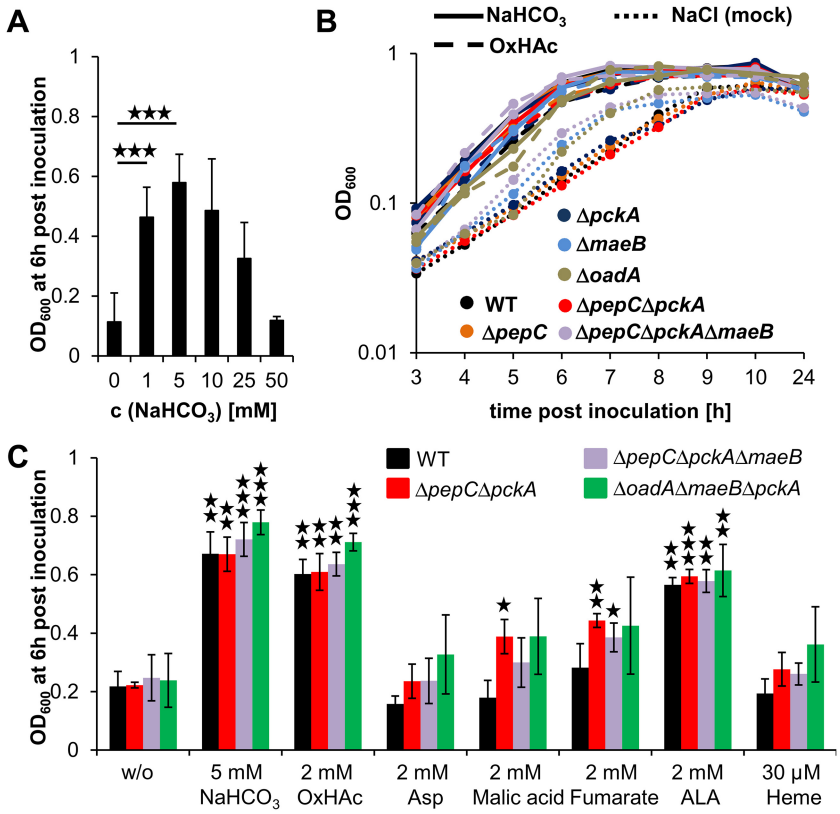

FIG 1 Growth of *A. pleuropneumoniae* in autoclaved PPLO medium. (A) Determination of the concentration-dependent effect of $NaHCO_3$ on growth of *A. pleuropneumoniae*. Bacteria were grown in autoclaved PPLO medium supplemented with glucose, NAD, and various concentrations of $NaHCO_3$ in closed tubes without shaking at 37°C. Bars represent mean OD_{600} values with standard deviations ($n = 5$) upon 6 h of growth. Three asterisks indicate a *P* value by Student's *t* test below 0.001. (B) Semilogarithmic presentation of growth curves of *A. pleuropneumoniae* wild-type (WT), Δ*pepC*, Δ*pckA*, Δ*maeB*, Δ*oadA*, Δ*pepC* Δ*pckA*, and Δ*pepC* Δ*pckA* Δ*maeB* strains upon supplementation of autoclaved PPLO medium (containing glucose and NAD) with 5 mM $NaHCO_3$, 2 mM oxaloacetic acid (OxHAc), or 5 mM sodium chloride for the indicated time. Symbols represent the mean OD_{600} values at the indicated time points postinoculation. For individual growth curves and number of replicates, see Fig. S3 in the supplemental material. (C) Growth of *A. pleuropneumoniae* wild-type (WT), Δ*pepC* Δ*pckA*, Δ*pepC* Δ*pckA* Δ*maeB*, and Δ*oadA* Δ*maeB* Δ*pckA* strains in autoclaved and additionally degassed PPLO medium (containing glucose and NAD) upon supplementation with either 5 mM $NaHCO_3$, 2 mM oxaloacetic acid, 2 mM aspartic acid, 2 mM malic acid, 2 mM sodium fumarate, 2 mM δ-aminolevulinic acid (ALA), or a solution containing 30 μM heme and 129 μM L-histidine. Bars represent mean OD_{600} values and standard deviations ($n = 3$) upon 6 h of growth. Statistics were performed by Student's *t* test comparing each supplemented sample to the negative-control (w/o) for each strain. *P* values below 0.05, 0.01, and 0.001 are indicated by one, two, or three asterisks, respectively.

revealing that growth of *A. pleuropneumoniae* in the presence of stable isotope-labeled $NaH^{13}CO_3$ led to incorporation of the ^{13}C carbon atom in total biomass of *A. pleuropneumoniae* ($\delta^{13}C \approx 250‰$). The incorporation of ^{13}C into total biomass was indistinguishable between the *A. pleuropneumoniae* wild type and the Δ*pepC*, Δ*pckA*, Δ*maeB*, Δ*oadA*, Δ*pepC* Δ*pckA*, and Δ*pepC* Δ*pckA* Δ*maeB* deletion mutants (Fig. 2C).

The fixed carbon atom is highly incorporated into aspartate and lysine. Analysis of the $^{13}C/^{12}C$ isotope ratios in amino acids by gas chromatography-combustion-isotope ratio mass spectrometry (GC-C-IRMS) showed incorporation of ^{13}C into aspartate ($\delta^{13}C \approx 5{,}000‰$) and to a lesser extent into lysine ($\delta^{13}C \approx 250‰$), whereas only minor ^{13}C enrichment was observed for alanine, glycine, glutamate, and valine ($\delta^{13}C \approx 10‰$). There was no difference between wild-type *A. pleuropneumoniae* and the Δ*pepC*, Δ*pckA*, Δ*maeB*, Δ*oadA*, Δ*pepC* Δ*pckA*, and Δ*pepC* Δ*pckA* Δ*maeB* deletion mutants with regard to ^{13}C isotope incorporation into amino acids (Fig. S4). Determination of $^{13}C/^{12}C$ isotope ratios in aspartate and lysine at different time points of growth of *A. pleuro-*

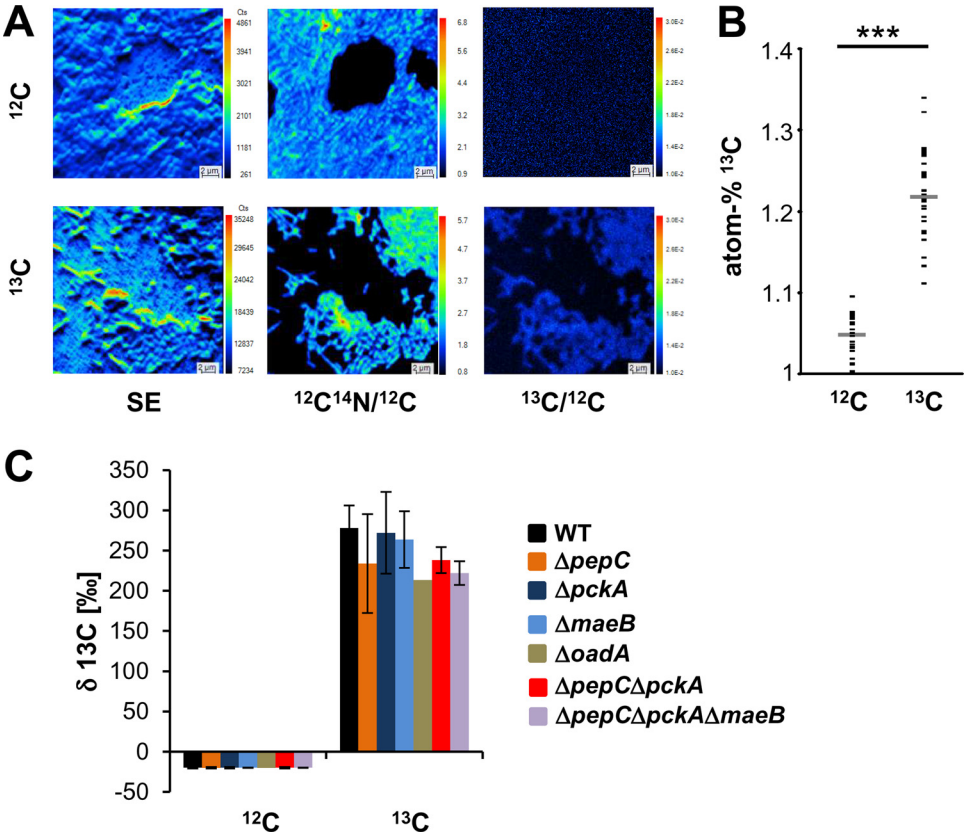

FIG 2 Fixation of carbon from $NaHCO_3$ by *A. pleuropneumoniae*. (A) NanoSIMS analysis of *A. pleuropneumoniae* grown for 6 h in the presence of either $NaH^{12}CO_3$ or $NaH^{13}CO_3$. Shown are secondary electron images (SE), $^{12}C^{14}N/^{12}C$ normalized images, and $^{13}C/^{12}C$ isotope ratio images. (B) Upon nanoSIMS analysis, 25 and 37 cells grown in the presence of $NaN^{12}CO_3$ or $NaH^{13}CO_3$, respectively, were randomly selected, and their atom% ^{13}C values were plotted. The mean values are depicted by the gray lines. Three asterisks indicate a *P* value by Student's *t* test below 0.001. (C) $^{13}C/^{12}C$ isotope ratios in total biomass of *A. pleuropneumoniae* wild-type (WT) ($n = 4$), Δ*pepC* ($n = 4$), Δ*pckA* ($n = 4$), Δ*maeB* ($n = 5$), Δ*oadA* ($n = 1$), Δ*pepC* Δ*pckA* ($n = 4$), and Δ*pepC* Δ*pckA* Δ*maeB* ($n = 3$) strains upon growth for 6 h in the presence of $NaH^{12}CO_3$ or $NaH^{13}CO_3$. Error bars represent standard deviations from at least three independent biological repeats.

pneumoniae in $NaH^{13}CO_3$-containing medium revealed that after a short lag phase of about 60 min, ^{13}C is incorporated rapidly within the following 80 min and reaches maximal values about 140 min after inoculation (Fig. 3A). The measured $^{13}C/^{12}C$ incorporation ratios in Asp and Lys could be perfectly fitted mathematically using the Chapman-Richards equation, $\Delta\delta^{13}C = a[1 - e^{(-bt)}]^c$ (27) (Fig. 3B), which is a sigmoid function that has been widely applied in biology to model cumulative growth behavior (27) and is based on Von Bertalanffy's growth theory (28). Applying GC-C-IRMS, we did not observe incorporation of $NaH^{13}CO_3$-derived ^{13}C into cellular fatty acids (Fig. S5).

***A. pleuropneumoniae* ΔpepC ΔpckA mutant is attenuated in infection.** As we could not delete PEPC in combination with the α subunit of OAD, we decided to test the double deletion mutant in which PEPC was deleted in combination with PEPCK (Δ*pepC* Δ*pckA* strain) in an animal infection experiment *in vivo*. Eight pigs were infected with wild-type *A. pleuropneumoniae* serotype 7 and its Δ*pepC* Δ*pckA* double deletion mutant. Two out of eight pigs of the group that had been infected with the *A. pleuropneumoniae* wild type had to be sacrificed during the first 3 days postinfection for reasons of animal welfare laws because of severe respiratory symptoms.

Body temperatures of pigs infected with the *A. pleuropneumoniae* Δ*pepC* Δ*pckA* strain were significantly lower on day 2 and day 3 postinfection than those of animals infected with the *A. pleuropneumoniae* wild type (Fig. 4A). Additionally, scores for clinical symptoms, lung lesions, and bacterial reisolation (Fig. 4B) were lower in the

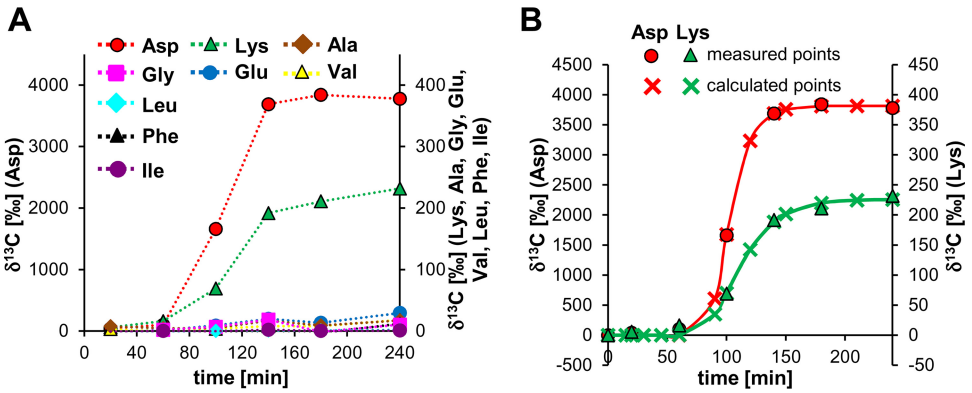

FIG 3 Incorporation of carbon from $NaHCO_3$ into amino acids by *A. pleuropneumoniae*. (A) Analysis of $^{13}C/^{12}C$ incorporation ratios for different amino acids at certain time points during growth of *A. pleuropneumoniae* wild type (WT) in medium containing $NaH^{13}CO_3$. (B) Mathematical fitting of incorporation ratios measured for Asp and Lys using the Chapman-Richards equation, $\Delta\delta^{13}C = a(1 - e^{(-bt)})^c$. Red circles and green triangles represent measured values, and red and green crosses that are connected by a line represent values calculated with the Chapman-Richards equation for Asp and Lys, respectively. In panels A and B, incorporation ratios for Asp refer to the primary (left) *y* axis, and all other amino acids refer to the secondary (right) *y* axis.

group infected with the *A. pleuropneumoniae* Δ*pepC* Δ*pckA* mutant but failed the significance threshold of a *P* value of ≤0.05. Assessment of CFU for the eight lung lobes, the lymph nodes, and the tonsils revealed that the *A. pleuropneumoniae* Δ*pepC* Δ*pckA* mutant could be reisolated from fewer tissue samples than the wild type (Fig. S6). No *A. pleuropneumoniae*-specific antibodies could be detected from serum samples obtained 1 week before infection. Three weeks after experimental infection, both groups showed a clear humoral immune response with no significant difference (Table 2).

DISCUSSION

Evolutionary adaptation of pathogens to their hosts is generally associated with a genome reduction (29) and a metabolism ideally suited to access the provided nutrient resources (30). The central metabolism of *A. pleuropneumoniae* resembles that of its related and likewise capnophilic and facultative anaerobic but nonpathogenic rumen bacteria *A. succinogenes* and *M. succiniciproducens* (10) for heterotrophic carbon fixation. Thus, we speculated that the obligate pathogen *A. pleuropneumoniae* uses bicarbonate or CO_2 from the blood buffering system as a carbon source during infection.

We showed that supplementation of PPLO medium that was degassed by autoclaving with 5 mM bicarbonate, which is at pH 7.4 in equilibrium with about 20-fold less CO_2 (31), was optimal to sustain *in vitro* growth of *A. pleuropneumoniae* in closed tubes. Under these conditions, the degassed medium becomes anaerobic because the growing bacteria rapidly consume the residual oxygen. At higher bicarbonate concentrations growth was impaired, which might be caused by the increased medium pH. However, we clearly demonstrated for the first time that *A. pleuropneumoniae* is able to heterotrophically fix carbon from bicarbonate and that the carbon atom is mostly incorporated into the oxaloacetate-derived amino acids aspartate and lysine (Fig. 5). As the carbon backbones of oxaloacetate and aspartate are identical, the carbon atom of the provided bicarbonate must have been already incorporated into oxaloacetate, which was not assessable with our analytical setup. This hypothesis is supported by the observed supportive effect on growth by either bicarbonate or oxaloacetic acid. Such fixation reactions occur at the PEP-pyruvate-oxaloacetate node and can directly give rise to oxaloacetate (8). However, we also observed a slight incorporation of the labeled carbon atom from bicarbonate into alanine, glycine, glutamate, and valine (Fig. 5), which might result from metabolic degradation products of the highly labeled amino acids Asp and Lys or from reversible flux through reactions of the central metabolism.

Based on homology, we identified the enzymes PEPC, PEPCK, MAE, and OAD in *A. pleuropneumoniae* that potentially catalyze carboxylation reactions at the PEP-

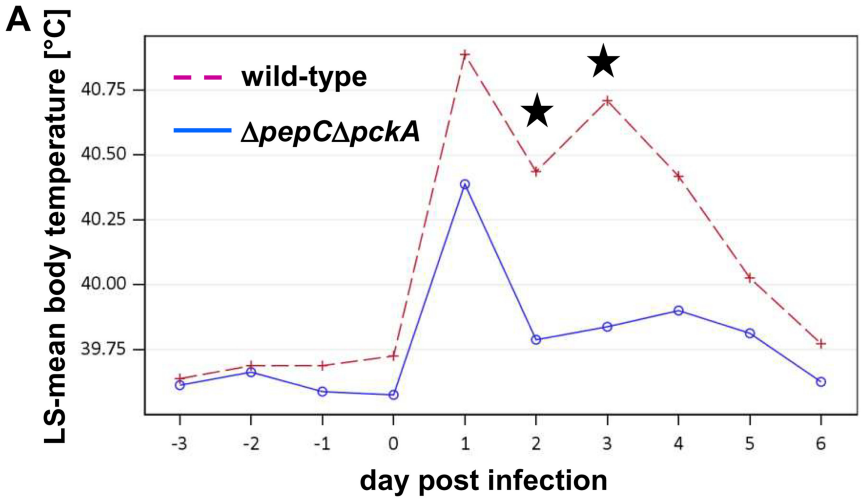

Type III Tests of Fixed Effects

Effect	Num DF	Den DF	F Value	Pr > F
Group	1	14	5.31	0.0371
Day	9	14	14.91	<.0001
Day*Group	9	14	3.31	0.0223

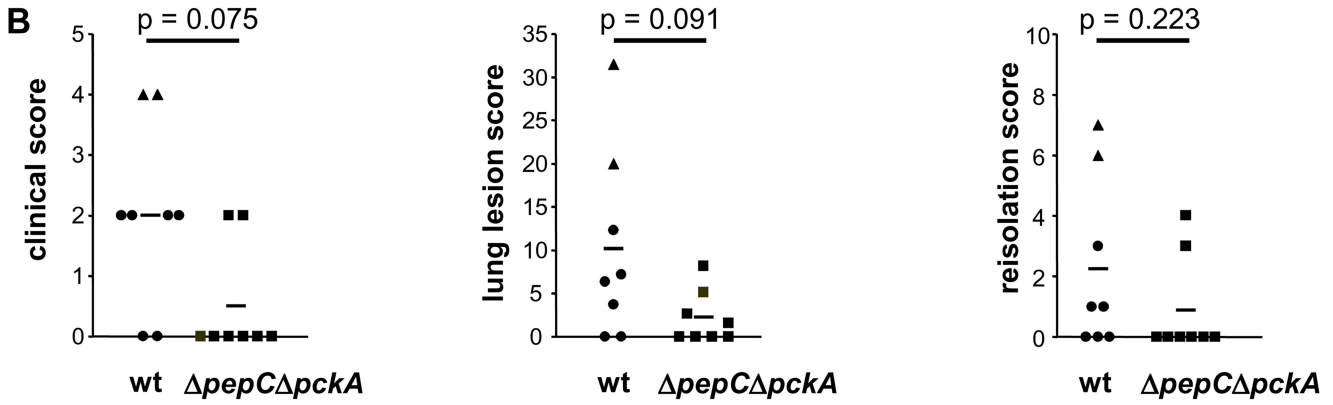

FIG 4 Analysis of *A. pleuropneumoniae* Δ*pepC* Δ*pckA* strain virulence using aerosol infection of pigs. (A) Time course of body temperature of animals infected with *A. pleuropneumoniae* wild-type or Δ*pepC* Δ*pckA* strain. Animals were infected on day 0. Body temperature was recorded starting 4 days before infection and during the following 6 days after experimental infection. Depicted are least-squares (LS) means of body temperatures within each group. A mixed-model repeated-measure analysis with group-day interaction revealed that the interaction between group and day is significant ($P = 0.0223$). *Post hoc* analysis was carried out regarding the combinations of fixed factors of interest, and significant differences on individual days are indicated by asterisks ($P < 0.05$ by Student's *t* test). Num DF, numerator degrees of freedom; Den DF, denominator degrees of freedom; F value, F value (test statistic); Pr > F, *P* value. (B) Clinical score, lung lesion score, and reisolation score (as indicated on the *y* axis) of pigs infected with *A. pleuropneumoniae* wild-type or Δ*pepC* Δ*pckA* strain. Each symbol represents one animal (triangles, two animals of the wild-type-infected group that had to be sacrificed within 3 days after infection because of animal welfare reasons; circles, six animals of the wild-type group that were sacrificed on day 21; rectangles, eight animals of the Δ*pepC* Δ*pckA* strain-infected group that were sacrificed on day 21). The horizontal lines represent the arithmetic means. Differences between *A. pleuropneumoniae* wild-type and Δ*pepC* Δ*pckA* strains were statistically analyzed using the Mann-Whitney U test and *P* values are depicted.

pyruvate-oxaloacetate node. Contrary to our expectations, deletion of their encoding genes and even combined deletion of *pepC*, *pckA*, and *maeB* did not affect bacterial growth kinetics or carbon fixation. However, it was not possible for us to delete *pepC* in combination with *oadA*. Based on their specific enzymatic activities,

TABLE 2 Virulence of *A. pleuropneumoniae* parent and Δ*pepC* Δ*pckA* mutant strain following aerosol challenge

Challenge strain	No. of animals	Challenge dose[a] (OD_{600}/cell no. [aerosolized] per 4 pigs)	Serological response to ApxIIA[b]	No. of animals with reisolation of *A. pleuropneumoniae* at postmortem analysis in:			
						Lung	
				Tonsil	Lymph node	Pneumonic	Intact
AP76	8	$0.434/1.9 \times 10^5$	38.3 ± 28.8	3	6	6	6
AP76 Δ*pepC* Δ*pckA*	8	$0.494/2 \times 10^5$	18.6 ± 21.8	0	2	4	4

[a]Bacteria were grown to the respective OD_{600} and diluted 1:15,000 with sterile saline; 13 ml of this dilution was aerosolized in the aerosol chamber.
[b]Recombinant ApxIIA protein was used as the solid-phase antigen as described previously (48); the number given is the arithmetic mean of the serum activity in enzyme-linked immunosorbent assay units.

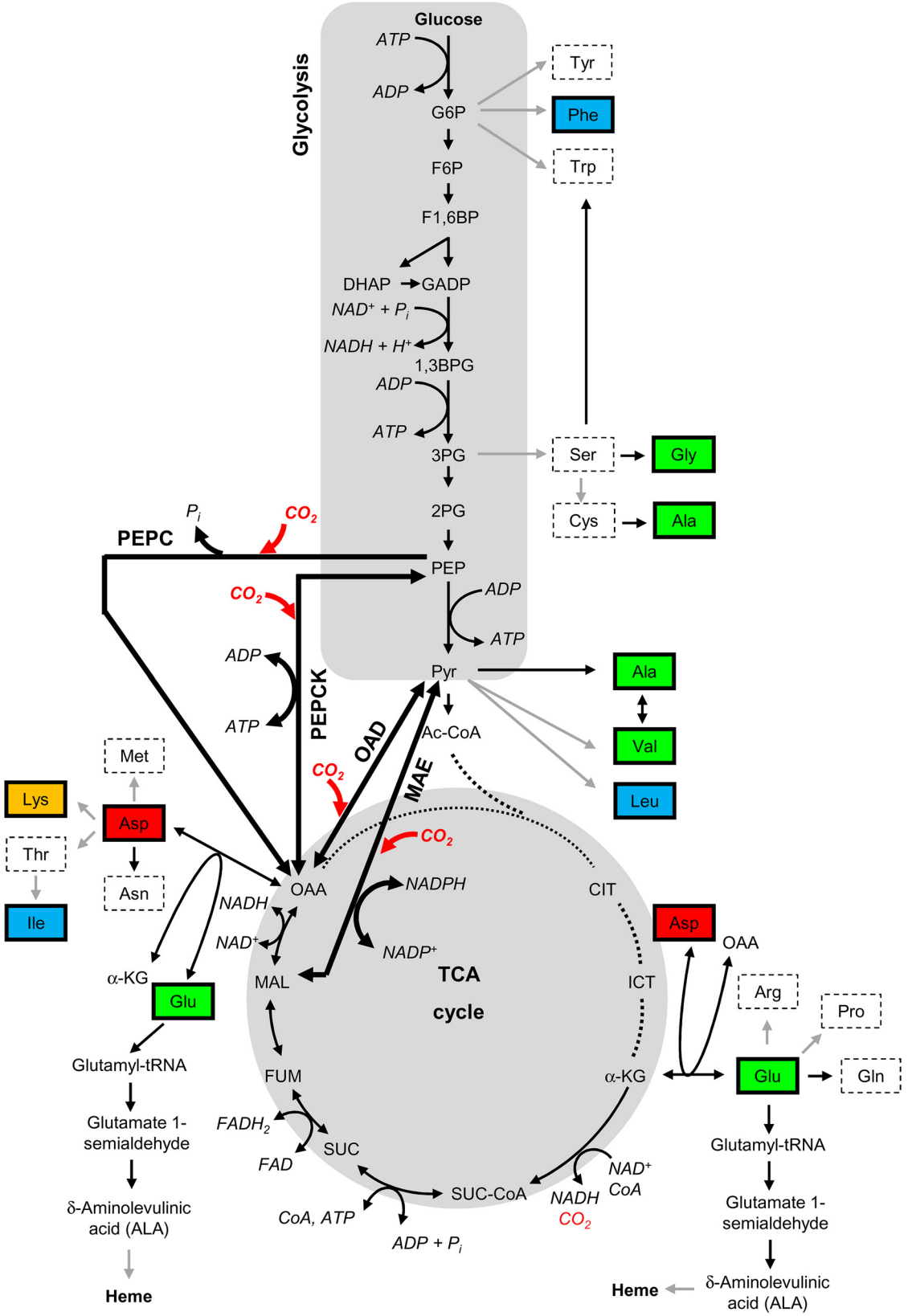

FIG 5 Scheme of glycolysis and reductive TCA cycle. Metabolites of glycolysis and TCA cycle and their contribution as precursors for amino acids are shown according to BioCyc for *E. coli* K-12 substrain MG1655 (www.biocyc.org). Metabolic pathways were deduced from the enzymatic repertoire of *A. pleuropneumoniae*, which is derived from the homology-based annotation of the *A. pleuropneumoniae* genome. Potential direct enzymatic interconversions are depicted by black arrows, and reactions including several steps are

(Continued on next page)

we hypothesize that PEPC and OAD are essential for carbon fixation in *A. pleuropneumoniae*, at least under the growth conditions tested. In accordance with our observation that growth of *A. pleuropneumoniae* is considerably reduced in the absence of bicarbonate or oxaloacetate, combined deletion of the potentially redundant enzymes PEPC and OAD might lead to impaired bacterial growth or even a lack of compatibility with viability of *A. pleuropneumoniae*, at least under our growth conditions. Bacteria frequently have multiple carbon-fixing enzymes at the anaplerotic node (8), which is probably a protection against spontaneous mutations that might render one or more of the enzymes nonfunctional. Moreover, it might be a strategy of the bacteria to rapidly adapt to changing environmental conditions due to differential regulation and different kinetics of the respective enzymes. Thus, we speculate that under our growth conditions the main flux of carbon into the reductive branch of the TCA cycle is mediated by PEPC and OAD of *A. pleuropneumoniae*.

A. pleuropneumoniae lacks several enzymes of the oxidative branch of the TCA cycle (7), and according to our model of central metabolism (Fig. 5), biosynthesis of numerous amino acids and TCA cycle intermediates depends on the reductive branch of the TCA cycle. These metabolites comprise precursors for synthesis of the iron-containing cofactor heme, which is essential for bacterial life (26, 32). We observed that the intermediate of heme biosynthesis, ALA, supported growth of *A. pleuropneumoniae* to an extent similar to that of bicarbonate or oxaloacetate, although it is far downstream of the carbon-fixing step. This finding suggests that carbon fixation at the PEP-pyruvate-oxaloacetate node is essential for the biosynthesis of heme under oxygen-deprived conditions, as in our culture system. A concentration of hemin that is used in a chemically defined medium for the related gammaproteobacterium *Haemophilus influenzae* (33) did not support growth of *A. pleuropneumoniae*. Hemin is poorly soluble in aqueous solution, and the applied concentration might be insufficient. However, we assume that carbon fixation and heme synthesis must also take place *in vivo*. Accordingly, *A. pleuropneumoniae* transposon mutants with insertional mutations in genes for synthesis of heme from glutamate showed a reduced *in vivo* and *in vitro* growth phenotype (34).

As we could not obtain a Δ*pepC* Δ*oadA* double deletion mutant of *A. pleuropneumoniae* and as PEPCK has been described in the related bacterial species *M. succiniciproducens* and *A. succinogenes* as most important for introducing C_3 metabolites of glycolysis into the reductive branch of the TCA cycle (10, 11), we instead decided to test the double deletion mutant of *pepC* and *pckA* of *A. pleuropneumoniae* in its natural porcine host. We observed that virulence of the *A. pleuropneumoniae* Δ*pepC* Δ*pckA* strain was reduced compared to that of its parental wild-type strain. Both PEPC and PEPCK seem to be of relevance during *A. pleuropneumoniae* infection. In support of our data, *pepC* expression is upregulated *in vivo* during the acute phase of the infection (35), and *pckA* is induced under the physiologically relevant condition of hypoxia (36, 37). According to our hypothesis that either PEPC or OAD is indispensable for carbon fixation, the poor *in vivo* expression of *oadA* (36) might be responsible for the observed

FIG 5 Legend (Continued)
shown by gray arrows. Double arrows indicate reactions that are potentially reversible. Enzymatic reactions that are probably missing in *A. pleuropneumoniae* are shown by dashed lines. Amino acids that could be analyzed by GC-C-IRMS are highlighted by boxes with solid lines. Depending on the degree of ^{13}C enrichments in amino acids, we applied the following color key: $\Delta\delta^{13}C$ [‰] ≈ 5,000, red boxes; $\Delta\delta^{13}C$ [‰] ≈ 250, orange boxes; $\Delta\delta^{13}C$ [‰] ≈ 10, green boxes; no enrichment, blue boxes. Amino acids that were not accessible with the analytical setup are shown in boxes with dashed lines. Potential carboxylation reactions by PEPC, PEPCK, MAE, and OAD are highlighted by boldface arrows. Abbreviations: G6P, glucose-6-phosphate; F6P, fructose-6-phosphate; F1,6BP, fructose-1,6-bisphosphate; DHAP, dihydroxyacetone phosphate; GADP, glyceraldehyde 3-phosphate; 1,3BPG, 1,3-bisphosphoglycerate; 3PG, 3-phosphoglycerate; PEP, phosphoenolpyruvate; Pyr, pyruvate; Ac-CoA, acetyl-coenzyme A (CoA); CIT, citrate; ICT, isocitrate; α-KG, α-ketoglutarate; SUC-CoA, succinyl-CoA; SUC, succinate; FUM, fumarate; MAL, malate; OAA, oxaloacetate; Tyr, tyrosine; Phe, phenylalanine; Trp, tryptophan; Ser, serine; Gly, glycine; Cys, cysteine; Ala, alanine; Leu, leucine; Val, valine; Arg, arginine; Glu, glutamic aicd; Gln, glutamine; Pro, proline; Asp, aspartic acid; Asn, asparagine; Met, methionine; Lys, lysine; Thr, threonine; Ile, isoleucine; PEPC, phosphoenolpyruvate carboxylase; PEPCK, phosphoenolpyruvate carboxykinase; OAD, oxaloacetate decarboxylase; MAE, malic enzyme.

attenuated phenotype in the *A. pleuropneumoniae* Δ*pepC* Δ*pckA* mutant. In accordance with our findings, recently it has been shown that anaplerotic fixation of CO_2 at the PEP-pyruvate-oxaloacetate-malate node is essential for intracellular survival of *Mycobacterium tuberculosis* (38). However, the nutritional state under *in vivo* conditions is largely unknown, and instead of carbon fixation, impaired decarboxylation of TCA cycle intermediates which can be catalyzed by PEPCK during gluconeogenesis might be responsible for the attenuation of the *A. pleuropneumoniae* Δ*pepC* Δ*pckA* mutant.

Taken together, in the porcine lung, PEPC and/or PEPCK is needed for the interconversion of C_3 and C_4 metabolites in order to generate essential TCA cycle or glycolysis intermediates, amino acids, and/or heme. The capability for heterotrophic carbon fixation seems to be evolutionarily selected in the obligate pathogenic bacterium *A. pleuropneumoniae* to access this carbon source within its porcine host (30). Based on our findings, we propose that the bicarbonate buffer or dissolved CO_2 in the blood play an underestimated role as an *in vivo* carbon source for pathogenic bacteria, and pharmacological targeting of bacterial enzymes involved in carbon fixation might provide a novel strategy for treatment of infection.

MATERIALS AND METHODS

Bacterial strains, plasmids, and primers. Bacterial strains, plasmids, and primers used in this study are listed in Table 1.

Media and growth conditions. *E. coli* strains were cultured in Luria-Bertani medium supplemented with the appropriate antibiotics and supplements (ampicillin, 100 μg/ml; chloramphenicol, 25 μg/ml; for *E. coli* 2155, 1 mM diaminopimelic acid [all from Sigma]). *A. pleuropneumoniae* strains were cultured at 37°C and 5% CO_2 in sterile-filtered PPLO medium or on PPLO agar (Difco) supplemented with 15 μM NAD (Merck), L-cysteine hydrochloride (260 μg/ml; Sigma), L-cystine dihydrochloride (10 μg/ml; Sigma), and 50 mM glucose (Roth). Selection of *A. pleuropneumoniae* transconjugants (single crossovers) was achieved by addition of chloramphenicol (5 μg/ml). The medium for counterselection was prepared as described previously (39). For cultivation of the complemented mutant, kanamycin (25 μg/ml) was added. To analyze the effects of bicarbonate on growth of *A. pleuropneumoniae*, PPLO medium was autoclaved and bottles containing hot medium were filled to the brim and tightly closed. The medium was supplemented with 15 μM NAD, 50 mM glucose, sodium bicarbonate (Roth), oxaloacetic acid (Sigma), aspartic acid (Sigma), sodium fumarate (Sigma), malic acid (Sigma), δ-aminolevulinic acid (Sigma), histidine (Calbiochem), or heme (Sigma). Stock solutions of oxaloacetic acid and malic acid were adjusted to neutral pH to avoid acidification of the medium. Fifty-ml samples of medium in screw-cap tubes (Sarstedt) were inoculated with consistent amounts of fresh *A. pleuropneumoniae* colony material from about 15-h-old plates. The tubes were tightly closed and incubated for the indicated time at 37°C without shaking. Purity testing of all growth experiments was performed by testing for growth on blood agar plates.

Construction of *A. pleuropneumoniae* deletion mutants. Construction of deletion mutants was performed as shown in Fig. S1 in the supplemental material (primers and plasmids are listed in Table 1). Briefly, the upstream and downstream parts of target genes were amplified from genomic *A. pleuropneumoniae* AP76 DNA, and the PCR fragments were cloned into pCR2.1-TOPO (Thermo Fisher Scientific). The upstream fragments were excised from the TOPO vector and cloned into the TOPO vector containing the downstream fragment, directly upstream of the latter, resulting in an in-frame deleted version of the respective gene. Subsequently the fused up- and downstream fragments were excised from the TOPO vector and cloned into the pEMOC2 vector, which was subsequently applied for the single-step transconjugation (40). In a first crossover, genomic integrates of the pEMOC2 vector were obtained, which were subsequently excised in a second crossover step, giving rise to the respective *A. pleuropneumoniae* deletion mutants. Deletion mutants were confirmed by PCR.

Isotope mass spectrometry and nanoSIMS. For determination of ^{13}C incorporation ratios in total biomass, individual cells, and amino and fatty acids, *A. pleuropneumoniae* was grown in PPLO medium supplemented with 5 mM sodium bicarbonate containing 99 atom% ^{13}C ($NaH^{13}CO_3$; Sigma). Inoculation and growth were performed as described above. Bacteria were harvested after 6 h by centrifugation at 13,000 × *g* for 5 min and washed with phosphate-buffered saline (PBS). Isotope ratios in total biomass were determined by EA-C-IRMS as described previously (41). Briefly, biomass was freeze-dried, combusted in an EA Fisons 1108 with CHN packing, and analyzed on a Finnigan MAT 252 isotope ratio mass spectrometer, and a mean isotope ratio was calculated from five repeats. Isotope ratios in total biomass were calculated according to the notation δ [‰] = $[(R/R_{PDB}) - 1] \times 10^3$, where R and R_{PDB} are the ^{13}C isotope ratios in the sample and the international standard Vienna PeeDee Belemnite (42). For determination of ^{13}C incorporation in individual bacterial cells, nanoSIMS was performed. Bacterial cells (^{13}C labeled or unlabeled) were fixed in 2% paraformaldehyde (PFA) at 4°C overnight and filtered on gold-palladium-coated polycarbonate filters (GTTP; pore size, 0.22 μm; Merck) (43), and samples were analyzed with a nanoSIMS 50L (Cameca). Areas of interest were presputtered with a Cs^+ primary ion beam of 200 pA to remove surface contamination, to implant Cs^+ ions in the sample, and to achieve an approximately stable ion emission rate. A primary Cs^+ ion beam with a beam current of around 2 pA and a beam diameter of <150 nm was rastered across the cells for analysis. For each area of interest,

secondary ion images of $^{12}C^-$, $^{13}C^-$, $^{12}C^{14}N^-$, and $^{32}S^-$ were simultaneously recorded from an analysis area range from 15 by 15 μm to 25 by 25 μm in size and an image size of 256 by 256 pixels with a dwell time of 1 ms per pixel. To minimize interference, the instrument was tuned for high mass resolution (around 8,000 mass resolution power). Images and data were processed using Look@nanosims freeware (44) based on Matlab. Determination of isotope ratios in amino acids and fatty acids was conducted by GC-C-IRMS using a Finnigan MAT 252 isotope ratio mass spectrometer as described previously (41, 45). For analysis of amino acids, biomass was treated with 6 M HCl (24 h, 100°C) to hydrolyze peptide bonds of proteins. Carboxyl groups were esterified and amino groups were acetylated (41). For fatty acid analysis, cells were saponified (15% [wt/vol] NaOH, 1 h, 100°C) and prepared for GC-C-IRMS as described earlier (45). Capillary gas chromatography was performed on a Hewlett Packard 5890 series II gas chromatograph equipped with a capillary column HP Ultra 2 and FID for amino acids, and fatty acids were separated with an Optima 5 column. Measured isotope ratios in amino acid and fatty acid derivatives were corrected for the isotope ratios in the derivatization reagents to obtain amino or fatty acid isotope ratios. A mean value for amino acid and fatty acid isotope ratios was calculated from triplicate measurements. For determination of isotope ratios in total biomass, amino acids or fatty acids from at least three independent biological replicates were analyzed.

Virulence studies. Virulence of the *A. pleuropneumoniae* Δ*pepC* Δ*pckA* mutant was analyzed and compared to that of the *A. pleuropneumoniae* serotype 7 wild-type strain by aerosol infection of swine, essentially as described previously (46), using an aerosol chamber built according to Jacobsen et al. (47). Sixteen *A. pleuropneumoniae*-free pigs (German Landrace; male, 7 to 9 weeks of age, no clinical symptoms of a respiratory disease and no serological response in the ApxII-enzyme-linked immunosorbent assay [48]) were randomly assigned to two groups of 8 animals each and cared for in accordance with the principles outlined by the *European Convention for the Protection of Vertebrate Animals Used for Experimental or Other Scientific Purposes* (European Treaty Series, no. 123 [http://conventions.coe.int/treaty/EN/treaties/html/123.htm] and 170 [http://conventions.coe.int/treaty/EN/treaties/html/170.htm]). *A. pleuropneumoniae* wild-type and Δ*pepC* Δ*pckA* strains were grown with shaking to an OD_{600} of about 0.4 to 0.5 and diluted 1:15,000 with sterile saline, and aerosol infection was performed with a challenge dose as specified in Table 2. Clinical examinations and scoring were performed as described previously (49). Briefly, the occurrence of coughing, dyspnea, and vomiting was monitored daily within the first 7 days postinfection. In order to quantify the results, a score of 1 was given for each of the symptoms, resulting in a maximum score of 3 per pig and day, which is in accordance with the specifications for the validation of *A. pleuropneumoniae* vaccines given in the European Pharmacopoeia (http://www.pheur.org). The animals were sacrificed on day 21 postinfection, and postmortem analysis, including determination of lung lesion scores (50) and bacterial reisolation, was performed as described by Baltes et al. (46). Briefly, each of the seven porcine lung lobes was scored separately. A score of 0 (healthy) to 5 (completely altered) was given, resulting in a maximum score of 35 per pig. This scoring system was adapted from the European Pharmacopoeia. For determination of the reisolation score, defined locations of each of the seven lung lobes were plated on selective meat blood agar (51). If either no bacteria were reisolated or growth occurred only in the area of the plate which had direct contact with the tissue sample, a score of 0 was given. Using a sterile loop, each sample was fractionated twice. A score of 1 was given if colonies were also present in the fractionated streaks. The reisolation score is the sum of the individual scores for each of the seven lung lobes. The identity of the challenge strain was confirmed by PCR. Statistical analyses were performed by using SAS for Windows, version 9.4 (SAS Institute Inc., Cary, NC, USA). A two-way mixed-model analysis of variance (between-subject factor, group; within subject factor, day) was used to study changes in temperature related to group (Δ*pepC* Δ*pckA* and wild-type strains), day, and group-day interaction. A general unstructured covariance structure was considered, and *post hoc* comparisons were performed by Student's *t* test. Nonparametric endpoints (clinical score, lung lesion score, and reisolation score) were evaluated by Mann-Whitney U test with exact approximation instead of a *t* approximation to consider the small sample size. *P* values of <0.05 were considered statistically significant.

SUPPLEMENTAL MATERIAL

Supplemental material for this article may be found at https://doi.org/10.1128/IAI.00768-18.

SUPPLEMENTAL FILE 1, PDF file, 2.2 MB.

ACKNOWLEDGMENTS

This work was supported by Sonderforschungsbereich 587 (project A4) of the Deutsche Forschungsgemeinschaft (DFG), Bonn, Germany.

We thank Tomas Vagner and Sten Littmann (Max Planck Institute for Marine Microbiology, Bremen, Germany) for the nanoSIMS analysis. We are grateful to Lothar Kreienbrock (University of Veterinary Medicine Hannover, Germany) for his help with biostatistical data analysis.

We have no competing financial or nonfinancial interests to declare.

REFERENCES

1. Fenwick B, Henry S. 1994. Porcine pleuropneumonia. J Am Vet Med Assoc 204:1334–1340.
2. Bossé JT, Janson H, Sheehan BJ, Beddek AJ, Rycroft AN, Kroll JS, Langford PR. 2002. *Actinobacillus pleuropneumoniae*: pathobiology and pathogenesis of infection. Microbes Infect 4:225–235. https://doi.org/10.1016/S1286-4579(01)01534-9.
3. Dom P, Haesebrouck F, Ducatelle R, Charlier G. 1994. In vivo association of *Actinobacillus pleuropneumoniae* serotype 2 with the respiratory epithelium of pigs. Infect Immun 62:1262–1267.
4. Baltes N, N'diaye M, Jacobsen ID, Maas A, Buettner FF, Gerlach GF. 2005. Deletion of the anaerobic regulator HlyX causes reduced colonization and persistence of *Actinobacillus pleuropneumoniae* in the porcine respiratory tract. Infect Immun 73:4614–4619. https://doi.org/10.1128/IAI.73.8.4614-4619.2005.
5. Buettner FF, Maas A, Gerlach GF. 2008. An *Actinobacillus pleuropneumoniae arcA* deletion mutant is attenuated and deficient in biofilm formation. Vet Microbiol 127:106–115. https://doi.org/10.1016/j.vetmic.2007.08.005.
6. Jacobsen I, Hennig-Pauka I, Baltes N, Trost M, Gerlach GF. 2005. Enzymes involved in anaerobic respiration appear to play a role in *Actinobacillus pleuropneumoniae* virulence. Infect Immun 73:226–234. https://doi.org/10.1128/IAI.73.1.226-234.2005.
7. Buettner FF, Bendallah IM, Bosse JT, Dreckmann K, Nash JH, Langford PR, Gerlach GF. 2008. Analysis of the *Actinobacillus pleuropneumoniae* ArcA regulon identifies fumarate reductase as a determinant of virulence. Infect Immun 76:2284–2295. https://doi.org/10.1128/IAI.01540-07.
8. Sauer U, Eikmanns BJ. 2005. The PEP-pyruvate-oxaloacetate node as the switch point for carbon flux distribution in bacteria. FEMS Microbiol Rev 29:765–794. https://doi.org/10.1016/j.femsre.2004.11.002.
9. Hong SH, Kim JS, Lee SY, In YH, Choi SS, Rih JK, Kim CH, Jeong H, Hur CG, Kim JJ. 2004. The genome sequence of the capnophilic rumen bacterium *Mannheimia succiniciproducens*. Nat Biotechnol 22:1275–1281. https://doi.org/10.1038/nbt1010.
10. McKinlay JB, Laivenieks M, Schindler BD, McKinlay AA, Siddaramappa S, Challacombe JF, Lowry SR, Clum A, Lapidus AL, Burkhart KB, Harkins V, Vieille C. 2010. A genomic perspective on the potential of *Actinobacillus succinogenes* for industrial succinate production. BMC Genomics 11:680. https://doi.org/10.1186/1471-2164-11-680.
11. Song H, Lee JW, Choi S, You JK, Hong WH, Lee SY. 2007. Effects of dissolved CO2 levels on the growth of *Mannheimia succiniciproducens* and succinic acid production. Biotechnol Bioeng 98:1296–1304. https://doi.org/10.1002/bit.21530.
12. Gokarn RR, Eiteman MA, Altman E. 2000. Metabolic analysis of *Escherichia coli* in the presence and absence of the carboxylating enzymes phosphoenolpyruvate carboxylase and pyruvate carboxylase. Appl Environ Microbiol 66:1844–1850. https://doi.org/10.1128/aem.66.5.1844-1850.2000.
13. Millard CS, Chao YP, Liao JC, Donnelly MI. 1996. Enhanced production of succinic acid by overexpression of phosphoenolpyruvate carboxylase in *Escherichia coli*. Appl Environ Microbiol 62:1808–1810.
14. Willenborg J, Huber C, Koczula A, Lange B, Eisenreich W, Valentin-Weigand P, Goethe R. 2015. Characterization of the pivotal carbon metabolism of *Streptococcus suis* serotype 2 under *ex vivo* and chemically defined *in vitro* conditions by isotopologue profiling. J Biol Chem 290:5840–5854. https://doi.org/10.1074/jbc.M114.619163.
15. McKinlay JB, Shachar-Hill Y, Zeikus JG, Vieille C. 2007. Determining *Actinobacillus succinogenes* metabolic pathways and fluxes by NMR and GC-MS analyses of 13C-labeled metabolic product isotopomers. Metab Eng 9:177–192. https://doi.org/10.1016/j.ymben.2006.10.006.
16. McKinlay JB, Vieille C. 2008. ^{13}C-metabolic flux analysis of *Actinobacillus succinogenes* fermentative metabolism at different $NaHCO_3$ and H2 concentrations. Metab Eng 10:55–68. https://doi.org/10.1016/j.ymben.2007.08.004.
17. Stretton S, Goodman AE. 1998. Carbon dioxide as a regulator of gene expression in microorganisms. Antonie Van Leeuwenhoek 73:79–85. https://doi.org/10.1023/A:1000610225458.
18. Passalacqua KD, Varadarajan A, Byrd B, Bergman NH. 2009. Comparative transcriptional profiling of *Bacillus cereus sensu lato* strains during growth in CO2-bicarbonate and aerobic atmospheres. PLoS One 4:e4904. https://doi.org/10.1371/journal.pone.0004904.
19. Bourgogne A, Thomson LC, Murray BE. 2010. Bicarbonate enhances expression of the endocarditis and biofilm associated pilus locus, *ebpR-ebpABC*, in *Enterococcus faecalis*. BMC Microbiol 10:17. https://doi.org/10.1186/1471-2180-10-17.
20. Caparon MG, Geist RT, Perez-Casal J, Scott JR. 1992. Environmental regulation of virulence in group A streptococci: transcription of the gene encoding M protein is stimulated by carbon dioxide. J Bacteriol 174:5693–5701. https://doi.org/10.1128/jb.174.17.5693-5701.1992.
21. Wong AC, Bergdoll MS. 1990. Effect of environmental conditions on production of toxic shock syndrome toxin 1 by *Staphylococcus aureus*. Infect Immun 58:1026–1029.
22. Iwanaga M, Yamamoto K. 1985. New medium for the production of cholera toxin by *Vibrio cholerae* O1 biotype El Tor. J Clin Microbiol 22:405–408.
23. Geers C, Gros G. 2000. Carbon dioxide transport and carbonic anhydrase in blood and muscle. Physiol Rev 80:681–715. https://doi.org/10.1152/physrev.2000.80.2.681.
24. Cummins EP, Selfridge AC, Sporn PH, Sznajder JI, Taylor CT. 2014. Carbon dioxide-sensing in organisms and its implications for human disease. Cell Mol Life Sci 71:831–845. https://doi.org/10.1007/s00018-013-1470-6.
25. Chen EY, Yang N, Quinton PM, Chin WC. 2010. A new role for bicarbonate in mucus formation. Am J Physiol Lung Cell Mol Physiol 299:L542–L549. https://doi.org/10.1152/ajplung.00180.2010.
26. Dailey HA, Dailey TA, Gerdes S, Jahn D, Jahn M, O'Brian MR, Warren MJ. 2017. Prokaryotic heme biosynthesis: multiple pathways to a common essential product. Microbiol Mol Biol Rev 81:e00048-16. https://doi.org/10.1128/MMBR.00048-16.
27. Pommerening A, Muszta A. 2015. Methods of modelling relative growth rate. Forest Ecosyst 2:5. https://doi.org/10.1186/s40663-015-0029-4.
28. von Bertalanffy L. 1957. Quantitative laws in metabolism and growth. Q Rev Biol 32:217–231. https://doi.org/10.1086/401873.
29. Moran NA. 2002. Microbial minimalism: genome reduction in bacterial pathogens. Cell 108:583–586. https://doi.org/10.1016/S0092-8674(02)00665-7.
30. Rohmer L, Hocquet D, Miller SI. 2011. Are pathogenic bacteria just looking for food? Metabolism and microbial pathogenesis. Trends Microbiol 19:341–348. https://doi.org/10.1016/j.tim.2011.04.003.
31. Kim Y, Massie L, Murata GH, Tzamaloukas AH. 2015. Discrepancy between measured serum total carbon dioxide content and bicarbonate concentration calculated from arterial blood gases. Cureus 7:e398. https://doi.org/10.7759/cureus.398.
32. Choby JE, Skaar EP. 2016. Heme synthesis and acquisition in bacterial pathogens. J Mol Biol 428:3408–3428. https://doi.org/10.1016/j.jmb.2016.03.018.
33. Coleman HN, Daines DA, Jarisch J, Smith AL. 2003. Chemically defined media for growth of Haemophilus influenzae strains. J Clin Microbiol 41:4408–4410. https://doi.org/10.1128/jcm.41.9.4408-4410.2003.
34. Sheehan BJ, Bossé JT, Beddek AJ, Rycroft AN, Kroll JS, Langford PR. 2003. Identification of *Actinobacillus pleuropneumoniae* genes important for survival during infection in its natural host. Infect Immun 71:3960–3970. https://doi.org/10.1128/iai.71.7.3960-3970.2003.
35. Deslandes V, Denicourt M, Girard C, Harel J, Nash JH, Jacques M. 2010. Transcriptional profiling of *Actinobacillus pleuropneumoniae* during the acute phase of a natural infection in pigs. BMC Genomics 11:98. https://doi.org/10.1186/1471-2164-11-98.
36. Klitgaard K, Friis C, Jensen TK, Angen O, Boye M. 2012. Transcriptional portrait of *Actinobacillus pleuropneumoniae* during acute disease–potential strategies for survival and persistence in the host. PLoS One 7:e35549. https://doi.org/10.1371/journal.pone.0035549.
37. Li L, Zhu J, Yang K, Xu Z, Liu Z, Zhou R. 2014. Changes in gene expression of *Actinobacillus pleuropneumoniae* in response to anaerobic stress reveal induction of central metabolism and biofilm formation. J Microbiol 52:473–481. https://doi.org/10.1007/s12275-014-3456-y.
38. Basu P, Sandhu N, Bhatt A, Singh A, Balhana R, Gobe I, Crowhurst NA, Mendum TA, Gao L, Ward JL, Beale MH, McFadden J, Beste D. 2018. The anaplerotic node is essential for the intracellular survival of Mycobacterium tuberculosis. J Biol Chem 293:5695–5704. https://doi.org/10.1074/jbc.RA118.001839.
39. Tonpitak W, Baltes N, Hennig-Pauka I, Gerlach GF. 2002. Construction of an *Actinobacillus pleuropneumoniae* serotype 2 prototype live negative-marker vaccine. Infect Immun 70:7120–7125. https://doi.org/10.1128/iai.70.12.7120-7125.2002.

40. Oswald W, Tonpitak W, Ohrt G, Gerlach G. 1999. A single-step transconjugation system for the introduction of unmarked deletions into *Actinobacillus pleuropneumoniae* serotype 7 using a sucrose sensitivity marker. FEMS Microbiol Lett 179:153–160. https://doi.org/10.1111/j.1574-6968.1999.tb08721.x.
41. Abraham WR, Hesse C. 2003. Isotope fractionations in the biosynthesis of cell components by different fungi: a basis for environmental carbon flux studies. FEMS Microbiol Ecol 46:121–128. https://doi.org/10.1016/S0168-6496(03)00203-4.
42. Craig H. 1957. Isotopic standard for carbon and oxygen and correction factors for mass-spectrometric analysis of carbon dioxide. Geochim Cosmochim 12:133–149. https://doi.org/10.1016/0016-7037(57)90024-8.
43. Musat N, Halm H, Winterholler B, Hoppe P, Peduzzi S, Hillion F, Horreard F, Amann R, Jorgensen BB, Kuypers MM. 2008. A single-cell view on the ecophysiology of anaerobic phototrophic bacteria. Proc Natl Acad Sci U S A 105:17861–17866. https://doi.org/10.1073/pnas.0809329105.
44. Polerecky L, Adam B, Milucka J, Musat N, Vagner T, Kuypers MM. 2012. Look@NanoSIMS–a tool for the analysis of nanoSIMS data in environmental microbiology. Environ Microbiol 14:1009–1023. https://doi.org/10.1111/j.1462-2920.2011.02681.x.
45. Abraham WR, Hesse C, Pelz O. 1998. Ratios of carbon isotopes in microbial lipids as an indicator of substrate usage. Appl Environ Microbiol 64:4202–4209.
46. Baltes N, Tonpitak W, Gerlach GF, Hennig-Pauka I, Hoffmann-Moujahid A, Ganter M, Rothkötter HJ. 2001. *Actinobacillus pleuropneumoniae* iron transport and urease activity: effects on bacterial virulence and host immune response. Infect Immun 69:472–478. https://doi.org/10.1128/IAI.69.1.472-478.2001.
47. Jacobsen MJ, Nielsen JP, Nielsen R. 1996. Comparison of virulence of different *Actinobacillus pleuropneumoniae* serotypes and biotypes using an aerosol infection model. Vet Microbiol 49:159–168. https://doi.org/10.1016/0378-1135(95)00184-0.
48. Leiner G, Franz B, Strutzberg K, Gerlach GF. 1999. A novel enzyme-linked immunosorbent assay using the recombinant *Actinobacillus pleuropneumoniae* ApxII antigen for diagnosis of pleuropneumonia in pig herds. Clin Diagn Lab Immunol 6:630–632.
49. Maas A, Jacobsen ID, Meens J, Gerlach GF. 2006. Use of an *Actinobacillus pleuropneumoniae* multiple mutant as a vaccine that allows differentiation of vaccinated and infected animals. Infect Immun 74:4124–4132. https://doi.org/10.1128/IAI.00133-06.
50. Hannan PC, Bhogal BS, Fish JP. 1982. Tylosin tartrate and tiamutilin effects on experimental piglet pneumonia induced with pneumonic pig lung homogenate containing mycoplasmas, bacteria and viruses. Res Vet Sci 33:76–88. https://doi.org/10.1016/S0034-5288(18)32364-6.
51. Jacobsen MJ, Nielsen JP. 1995. Development and evaluation of a selective and indicative medium for isolation of *Actinobacillus pleuropneumoniae* from tonsils. Vet Microbiol 47:191–197. https://doi.org/10.1016/0378-1135(95)00062-F.
52. Anderson C, Potter AA, Gerlach GF. 1991. Isolation and molecular characterization of spontaneously occurring cytolysin-negative mutants of *Actinobacillus pleuropneumoniae* serotype 7. Infect Immun 59:4110–4116.
53. Dehio C, Meyer M. 1997. Maintenance of broad-host-range incompatibility group P and group Q plasmids and transposition of Tn5 in Bartonella henselae following conjugal plasmid transfer from Escherichia coli. J Bacteriol 179:538–540. https://doi.org/10.1128/jb.179.2.538-540.1997.
54. Baltes N, Hennig-Pauka I, Jacobsen I, Gruber AD, Gerlach GF. 2003. Identification of dimethyl sulfoxide reductase in *Actinobacillus pleuropneumoniae* and its role in infection. Infect Immun 71:6784–6792. https://doi.org/10.1128/iai.71.12.6784-6792.2003.